Nanofabrication on insulating substrates

Electron beam lithography on quartz

Trabajo de Fin de Máster: Física y Tecnologías Físicas

por

Francisco Freire Fernández

Directores: José María de Teresa Nogueras

Soraya Sangiao Barral

Departamento de Física de la Materia Condensada

Contents

1 Introduction

1.1 Thesis motivation

Electron Beam Lithography (EBL) is a fundamental technique used in nanofabrication, allowing the direct writing of structures down to sub-10nm dimensions. Derived from the early Scanning Electron Microscopes (SEM), the technique briefly consists of scanning a beam of electrons accross a surface covered with a resist film sensitive to those electrons and energy is deposited in the desired pattern in the resist film. Depending on the resist nature, positive or negative tone, exposed or unexposed regions are removed in the development step, respectively. Fig.1 sketchs out the main steps involved in a EBL process. Nanoimprint lithography, deep, and extreme ultraviolet lithography are examples of high volume nanoscale patterning technologies which rely on EBL as a basic tool for the creation of the masks and the templates that they use.

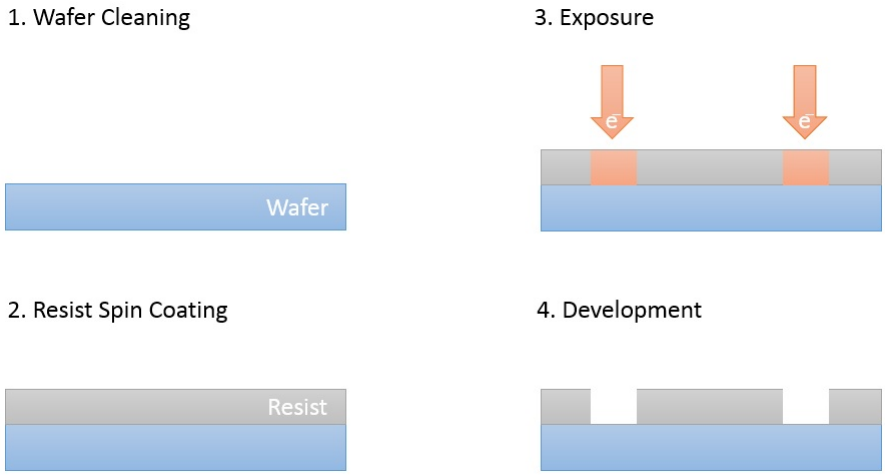

Figure 1: Sketch of the basic steps a EBL process consists of: 1º sample cleaning, 2º positive tone resist spin coating, 3º exposure of the resist, 4º design development, i.e., removal of the EBL products.

However, EBL applicability to insulating substrates remains challenging because of surface charging effects. Unlike patterning on conducting substrates where the charge excess is dissipated as the beam passes through the resist, patterning on insulating samples results in charge trapping near the surface. This charge accumulation (Fig.2) produces an unbalanced suface potential of the resist that deflects the beam and causes severe pattern distortions.

To overcome this problem, the most widely used anti-charging method is to coat the resist with a thin metal or conducting polymer layer to dissipate the charge. Similar to variable pressure scanning electron microscopy, variable pressure EBL [1] has demonstrated the capability of conducting EBL on insulating substrates since the negatively-charged electrons can be balanced by the positive ions created by the electron-gas molecule collisions; yet, the resolution may suffer from the electron scattering by the gas molecules. Another charging dissipation technique is the Critical Energy EBL (CE-EBL), which makes use of the fact that at certain electron energy the number of ejected electrons (secondary and backscattered) is equal to the injected primary electrons, leading to the suppression of the charging effect. In addition, charging distortion can be prevented by carring out the EBL on a thin electron-transparent membrane that traps only a small percentage of the electrons [2].

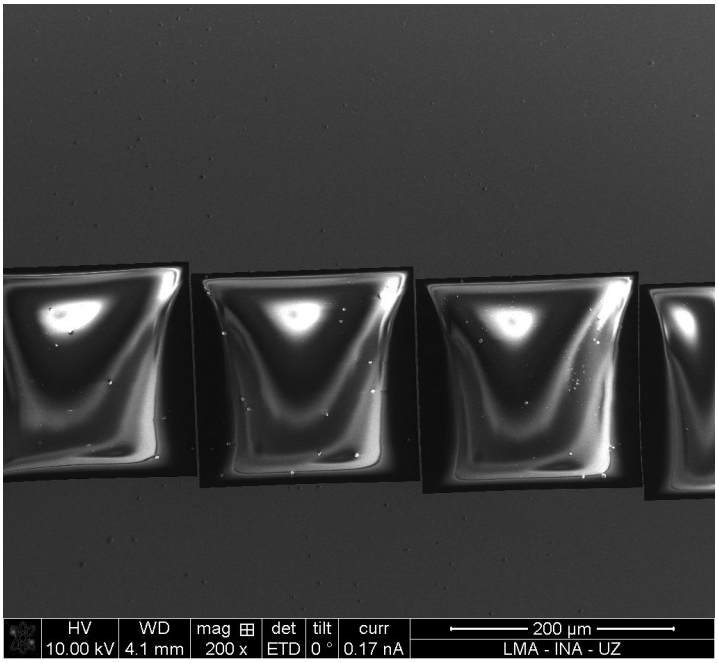

Figure 2: SEM image of a quartz substrate coated with an Au layer; EBL squares were exposed, only quartz remains in those regions. This image shows the charge accumulation on the insulating areas of the sample. Whereas the Au layer, that is connected to ground, efficiently evacuates the charge excess.

In this text we will study the use of charge conducting layers (on top and underneath of the resist layer) and the CE-EBL method to fabricate nano-optical devices such a standard and sub-wavelength metal difraction gratings and subwavelength appertures arrays. The characterization of these devices will be done using a Fourier Transform InfraRed (FTIR) system, which provides transmittance and reflectance measurements.

A sub-wavelength grating (SWG), which has a smaller period than the wavelength of an incident light, does not generate higher diffraction orders. When the grating period is much smaller than the wavelength ($\approx \lambda/10$), the grating behaves as a homogeneous layer with effective refractive index between the material index and the surrounding index which depends on the polarization of the incident light. Applications of SWGs today include antireflection filters[3-4] and phase plates[5].

The optical properties of subwavelength apertures in metallic films have been the focus of much research activity since the extraordinary optical transmission (EOT) phenomenon [14]. EOT is an optical phenomenon in which a structure containing subwavelength apertures in an opaque screen transmits more light than might naively be expected on the basis of either ray optics or even knowledge of the transmission through individual apertures. Surprisingly, such arrays may, for certain wavelengths, exhibit transmission efficiencies (normalized to the total area of the holes) that exceed unity. In other words, for these wavelengths a periodic array of subwavelength holes transmits more light than a large macroscopic hole with the same area as the sum of all the small holes.

1.2 Master's thesis outline

The Master's thesis is organized as follows. First, an introduction to the EBL on insulating substrates problem and applications is presented. Section 2 compiles and describes the experimental equipment utilized in the fabrication and characterization processes. Thereupon, EBL on insulating substrates is treated in Section 3. Once the sample preparation is introduced and the problem origin and solutions are stated, in Section 4 we will show the results obtained and will delve deeper into the different approaches followed. Finally, Section 5 will highlight the drawbacks and advantages of each method. Further details of minor points have been presented in the form of appendices.

2 Facilities & Equipment

In this section we will review the different equipment and techniques used throughout the fabrication process and the characterization of the optical-devices. The fabrication process took place in the clean room facilities at the Advanced Microscopy Laboratory (LMA) while the characterization mesurements within the facilities of the Nanoscience Insitute of Aragón.

The entire work presented is experimentally based on EBL on quartz samples, which play the role of a stantdard insulator. This material comes in 4" wafers which are cut into 1 $cm^2$and 49 mm^2square samples. Depending on the EBL technique employed, the first step on the fabrication process is the spin of the resist layer.

2.1 Resist spin-coating

In order to minimize the defect level, this process takes place in a class 100 cleanroom. The first step is to assure the best surface adherence conditions for the resist we are about to use. Secondly, we have to carefully design and execute a recipe which will produce the best resist layer properties required by our process. The last and most important step is the prebake (softbake) of the resist.

The surface preparation of the samples consists of a cleaning step. Here, the goal is a proper elimination of any type of surface contamination (especially, the resist used during the wafer cutting process) . In order to complete this task, the samples are inmersed in acetone and placed in an ultrasonic bath for three minutes at room temperature. The same process is repeated using isopropanol instead of acetone and then, a deionized water rinse and N_2-dry follows. Further cleaning could be achieved using O_2-plasma ashing, but for our purposes it is not necessary.

The resist used is a positive tone PMMA E-Beam Resist AR-P 679.04 provided by ALLRESIST GmbH. This polymer has a high molecular weight, 950K[1], which means that it is 20% less sensitive than the same product with a molecular weight of 50K and therefore higher doses would be required during EBL exposures. The resist thickness of this product ranges from 630 nm at a spin speed of 1000 rpm to 220 nm at 6000 rpm (spinning time 60 seconds). As we will later discuss, the different fabrication processes involve different resist thicknesses, which will also determine the metal layer thickness that we could later evaporate. However, the only positive tone resist avaible was the one quoted and its thickness range has constrained and determined the fabrication process. Besides the characteristics discussed, there are other parameters like the glass temperature, casting solvent, etc. that are fundamental in the coating process; we will introduced them as we described the following steps.

Spin coating is the dominant and most reproducible resist coating process. This technique encompasses the dynamics of centrifugal forces, the rheology of viscous polymers, and the dynamics of solvent transport. Empirically, the spin speed versus thickness curve is paramentric (Fig.3) and linear on a log-log scale. It

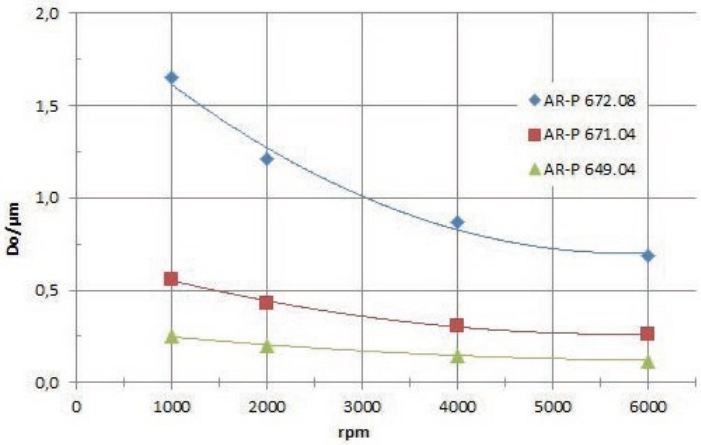

Figure 3: Resist spin curve [6].

is not just the spin speed that determines the film thickness, but also the nature of the casting solvent. Low-boiling solvents (e.g., acetone) produce thick and cloudy films due to the absoption of water and the precipitation of the polymer from the solvent. Thus, laminar air flow is used to evaporate more solvent and

[1] 950000 $\frac{g}{mol}$

to produce thicker films. Since saturating the vapor with solvent produces thinner films, the evaporation of the solvent controls the final film thickness. If there were no evaporation[2], then after the centrifugal forces had leveled the film, the film thickness would decrease to zero thickness with continued spinning. Fig.4 shows the spin coating equipment used. High resolution was sought in our designs, therefore we

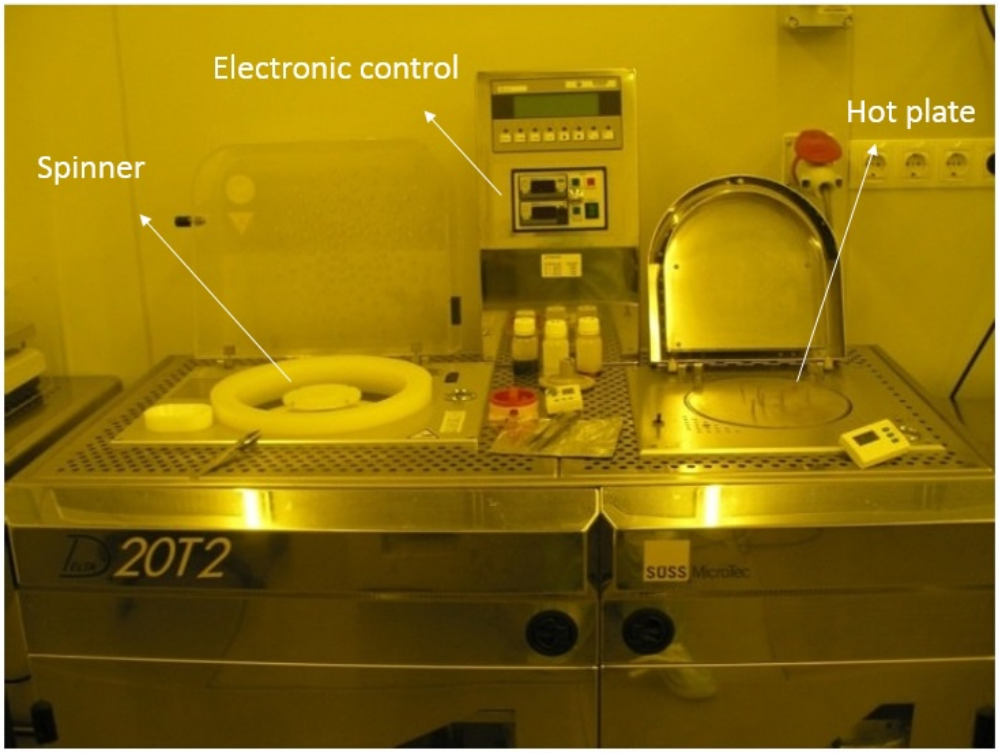

Figure 4: Spinner and hot plate equipment.

were interested in the minimun thickness the resist could provide. Consequently, the resist was spun at 6000 rpm, the total spinning time being of 60 seconds[3].

2.2 Softbake

The next step is called softbake or prebake. Softbake is the physical process of conversion of a liquid-cast resist into a solid film. This process involves the physical removal of the casting solvent without the degradation of the resist components. By removing the casting solvent from the film, a solid state is formed which prevents mixing of the exposure products with the unexposed zone.

Softbake should be precise as exposure and development of the image vary according to this process. If the softbake is too high, the radiation-sensitive component may be partially degraded, and higher doses will be required. If the softbake is too low, the casting solvent may interface with the radiation chemistry and different exposure-developer combinations may be required.

In drying a film consisting of a polymer, sensitizer, and solvents, the efficiency of solvent removal and the upper softbake temperature are determined by several physical and chemical factors. The T_g (glass transition temperature, PMMA: $T_g = 105^{o}$) and the T_d (decomposition temperature, PMMA: $T_d = 200^{o}$) of any components determine a practical upper limit. For efficient solvent removal, the softbake temperature should be above the T_g of the polymer, but should not be high enough to decompose the radiation-sensitive components. Secondly, the softbake temperature, if possible, should be above the boiling point of the casting solvent; ethyl lactate with a boiling tempreture of 155^{o}C is the solvent of the resist used. Taking into account all the previous data, the softbaking temperature choosen was 165^{o}C. The heating process took place on a hot plate (shown in Fig.4) and lasted for 2.5 minutes[4].

[2] Evaporation does not become significant until 10 sec has elapsed.

[3] The reason why the resist is spun during 60 sec is because, in matter of seconds, the solvent evaporates from a very thin film and the solid concentration reaches its final value where flow has ceased completely, due to the high viscosity. At this stage, about 30% of the solvent is left and then slowly dries.

[4] The softbake time is defined as the necessary time to evaporate 100% of the casting solvent. However, there is no

2.3 Conducting layer

The deposition of the conducting layer is determined by the EBL approach chosen. Obviously, if the conducting layer is underneath the resist film, this process will take place before the resist coating of the surface. In the case of CE-EBL this step is omitted. The metal film is evaporated in a BOC Edwars Auto 500 electron-beam evaporation system (Fig.5).

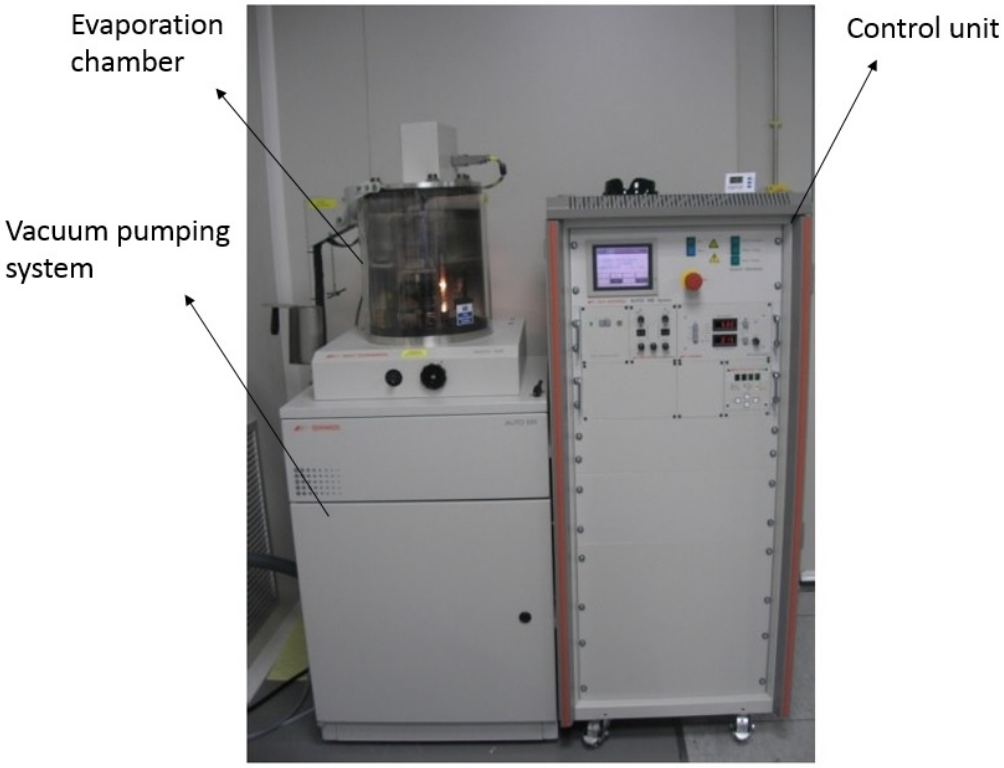

Figure 5: BOC Edwars Auto 500 electron-beam evaporation system.

This system generates and deflects an e-beam aiming at a metal target. Evaporation is achieved and the metal ions are deposited onto the sample surface. This technique enables ultra pure films deposition of materials with high melting points, and other materials that are difficult to deposit or control by resistance evaporation. At the first, sputtering was a better technique for this purpose, since it is faster than e-beam evaporation and does not require ultra high vacuum. However, 7nm Al coatings did not produce the effect desired. Resistance measurements revealed that the film deposited through this technique tend to oxidise very quickly and Al_2O_3 was formed on top of the resist and therefore no charge dissipation was accomplished. E-beam evaporated films did not present this problem.

Au and Al were the metals selected to work with in the conducting layer approach. When the conducting layer was placed on top of the resist, the film thickness was 6 to 7 nm in the case of Al, and later was found that 10 nm Au films also fulfilled the purpose. On the other hand, when the film was deposited underneath the resist layer, the thickness varied between 50 nm and 175 nm for both materials. We will cast light on this thickness difference later when we discuss the EBL approaches taken.

2.4 Electron Beam lithography

Once the sample is ready for the EBL approach chosen, the next step is its application. Here, we will only introduce the equipment, and further details about the technique will be given in the following sections.

The EBL system consists of a combination of a Raith Elphy Plus pattern generator attachment and a Dual Beam (FIB-SEM) Helios 600 from FEI. The Raith attachment allows the design of a wide variety of strucutres and presents Proximity effect correction among other interesting functionalities. From the point

experimental way to measure this in the Insititute facilities. For that reason, according to the supplier's advice, the time was choosen to be the one mentioned.

of view of the pattern generator, the designs are broken down into basic exposure units[5] and converted into 16-bit Digital Analogic Conversion (DAC) steps. The exposure of a certain element is characterized by the dwell time per DAC step, τ_{Dwell}, and the number of DAC steps the element is made of. When the exposure begins, the pattern generator takes control under the (electrons column) beam blanker, and dual DAC addresing for X and Y beam deflection takes place at a speed of 12 MHz.

The FEI system offers the user a large range of currents and e-beam acceleration voltages ranging from a few pA to 22 nA and from 1 keV to 30 keV, respectively. Different combinations of these parameters are needed by the different EBL methods which will be specified in the context of each one.

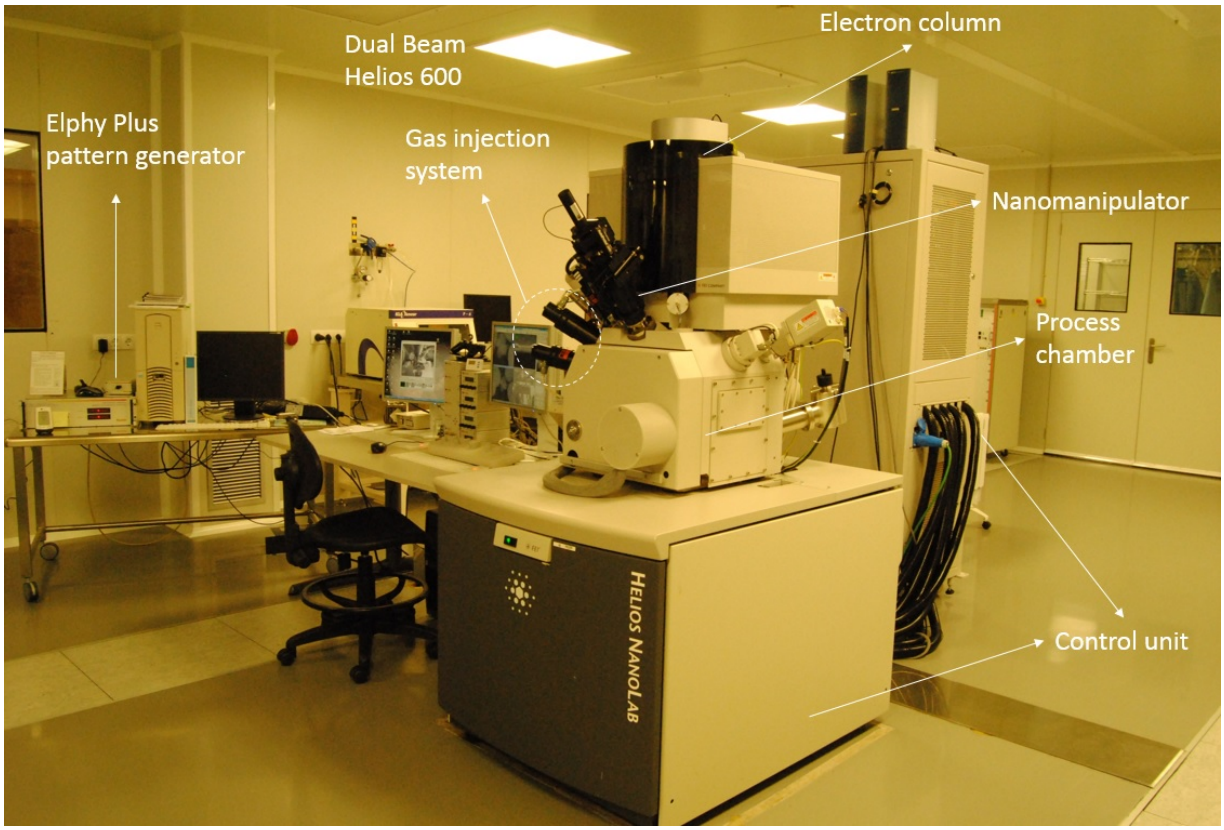

Figure 6: From left to right we presented the Elphy Plus pattern generator from Raith and the Helios 600 Dual beam system from FEI.

2.5 Development

After the EBL exposure has finished, the resist development is the next step. If a conducting layer on top of the resist was used, this is removed applying the proper wet etching process. In the case of an Al conducting layer an AZ developer was employed. The sample is immersed in the chemical for 3 minutes and rinsed in dionized water. Similarly, in the case of Au, a $(5\%)I_2 + (10\%)KI + (85\%)H_2O$ was applied for 2 mins and washed out in dionized water.

The exposure process induces chemical changes in polymers such as random scission or cross-linking and molecular rearrangements in small molecules added to polymers. The chemical products are distinguished from the unexposed reactants by a developer or process of development. The object of the development step is to remove the exposed resist region at a faster rate than the background in a reproducible, controlled manner. In the case of PMMA, the primary radiation event is the scission of the main chain and ester group.

The developer available is a methyl isobutyl ketone (MIBK) disolution provided by ALLRESIST under the name of AR-600-56. According to the supplier, the resist used must be developed in this product for 3 minutess followed by a 30 seconds stopping process in IPA; this is what was done.

[5] The dimensions of these basic units depend on the raster size which is determined by the writefield size; the smallest raster size is 2nm and this increase in 2 nm steps.

2.6 Specific processes

The development of the structures patterned puts an end to the main processing chain. Once this is complete, different paths are taken in the optical-devices fabrication process.

When the CE-EBL and the conducting layer (on top of the resist) methods are applied, a PMMA mask on top of the substrates is formed. Then, a metal layer is evaporated on top of the mask and the resist is removed through a lift-off process. The samples designated for this purporse were metal coated on the e-beam evaporator and Al was the metal employed in the lift-off process. Further details will be given when discussing the results of these EBL techniques.

Regarding the third approach, the PMMA mask is placed on top of the metal layer that will be part of the optical-devices. Now, instead of a lift-off process, it is the metal layer which is eroded in an ion milling process. Afterwards, the remaining resist layer is removed through O_2 plasma ashing.

2.6.1 Ion milling

In the ion milling process, an Ar plasma is created in a vacuum chamber, which contains a constant flow of Ar gas at reduced pressure typically around 1 mbar. The gas is exposed to a radio frequency potential resulting in the partial gas ionization. Thus, Ar^+atoms act like an ion beam aiming at the sample surface. As the atoms strike the surface, the surface is homogeneously eroded.

The equipment utilized was a SISTEC system built according to INA specifications (Fig.7)

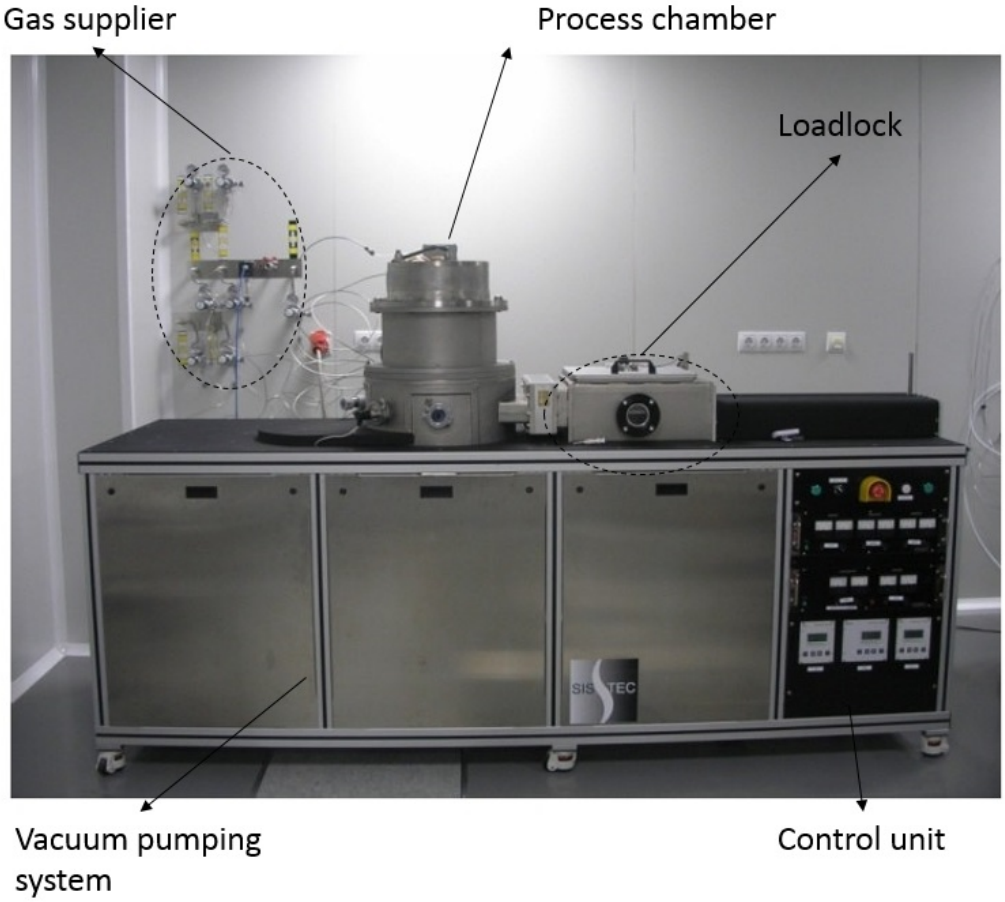

Figure 7: SISTEC RIE and ion milling system.

which allows the application of reactive ion etching (RIE) and ion milling.

In order to properly apply this technique, first we had to measure the ion milling rates of the materials involved (see Appendix I). For our working conditions[6], the ion milling rates are 22.5 nm/min , 12.5 nm/min, and 5 nm/min for Au, PMMA and Al, respectively.

[6] In the ion milling process the Ar gas flow is of 6 sccm, the ion beam power unit works at 250V, 100mA and the RF applied is of 205W.

2.6.2 O_2 plasma ashing

Resist removal becomes challenging when the resist has gone through different processes. In this context, O_2 plasma ashing is the most effective technique, providing excellent results at a rate of 10 nm/min. Similar to the ion milling technique, an oxygen plasma is generated in a vacuum chamber. The resist removal is assisted by O_2 molecules and the heating of the sample to 100ºC. Of course, only samples with Au coatings are subjected to this removal technique. In the case of Al coatings, wet etching of the resist is the only method available which will not alter the metal film.

The rate mentioned above is achieved using an O_2 pressure of 0.3 mbar at an O_2 gas flow of 50 sccm, heating the sample to 100ºC and applying an RF power of 150W. Again, the equipment is a SISTEC plasma enhanced chemical vapor deposition (PECVD) system built according INA specifications, Fig.8

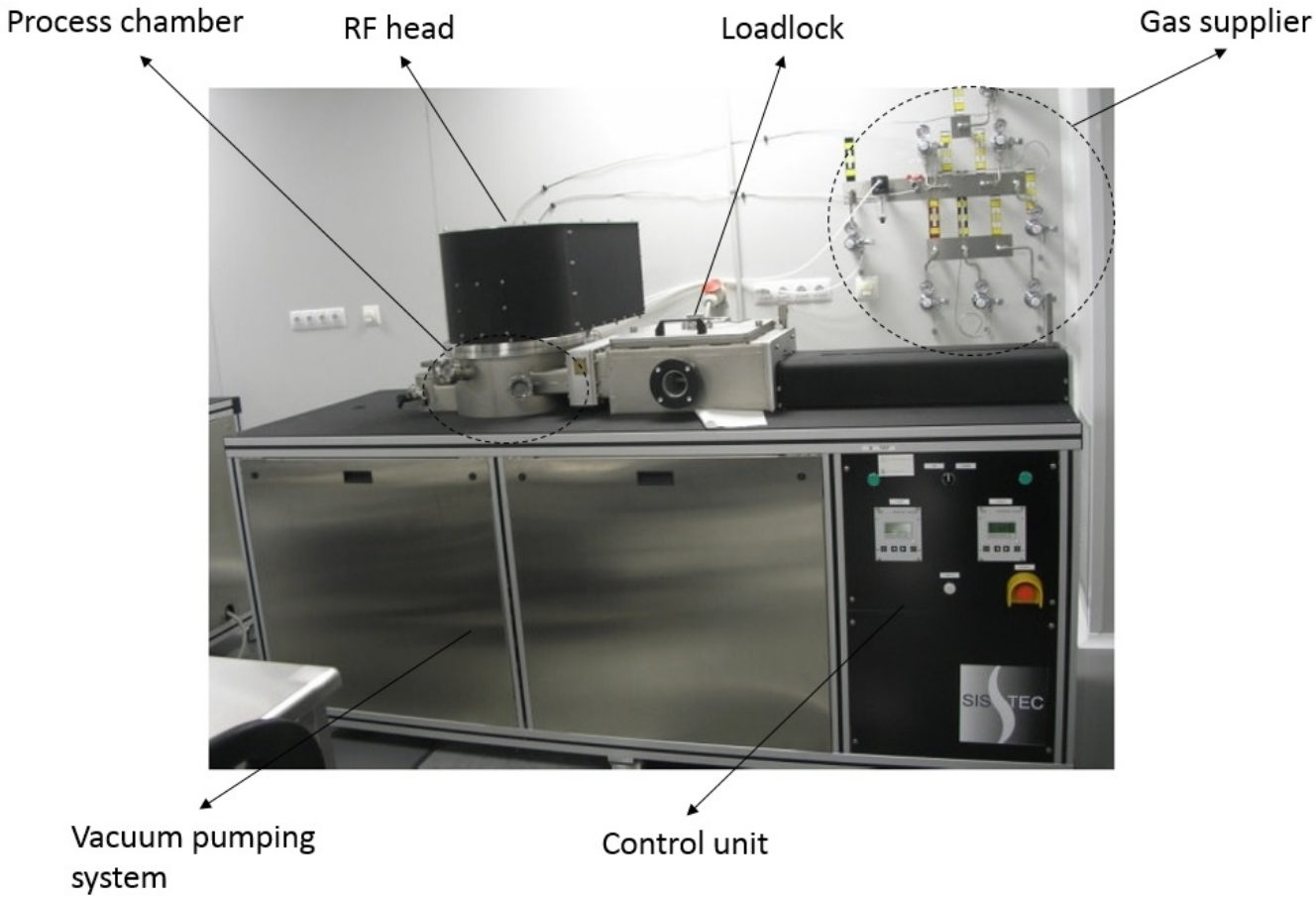

Figure 8: SISTEC PECVD system.

.

2.7 Reflectance & transmittance measurements

Although infrared spectroscopy and Fourier transformed infrared spectroscopy (FTIR) are techniques that have their primary application in organic chemistry, FTIR spectroscopy is an ideal technique to characterize the transmittance and reflectance of the devices fabricated. The system (Fig. 9)

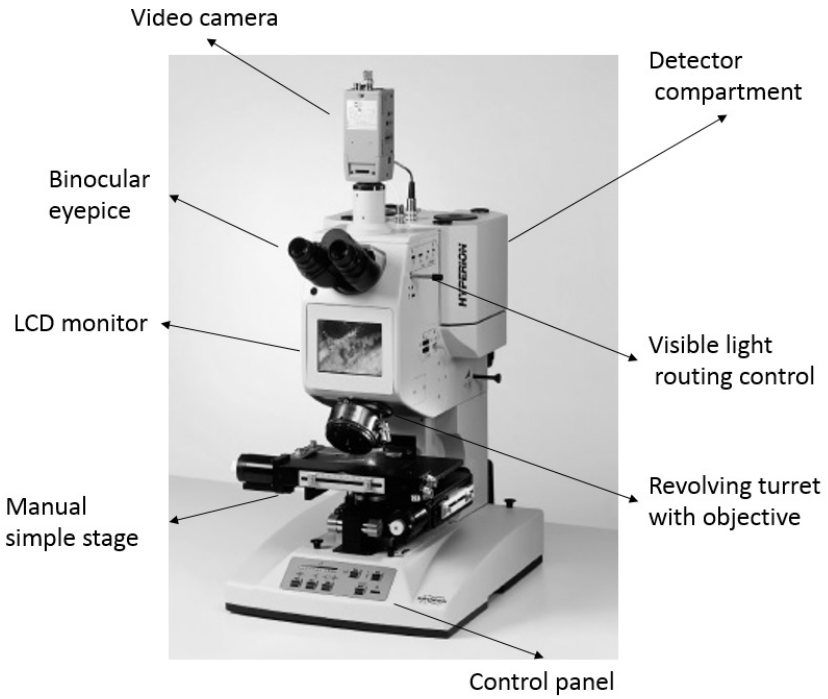

Figure 9: Bruker Hyperion 2000 FTIR system.

is a Bruker Hyperion 2000 which covers the wavelength range from 1.2μm to 20μm.

Roughly speaking, the technique emcompasses the following instrumentation: a source, an interferometer, and a detector. The light coming out of the source passes through the beamsplitter of a Michelson type interferometer and sends light in two directions at right angles. One beam goes to a stationary mirror and then back to the beamsplitter and the other goes to a moving mirror. The motion of the mirror makes the total path length variable versus that taken by the stationary-mirror beam. When the two meet up again at the beamsplitter, they recombine, but the difference in path lengths creates constructive and destructive interference leading to an interferogram. Then, the recombined beam passes through the sample. The sample absorbs all the different wavelengths characteristic of its spectrum, and this substracts specific wavelengths from the interferogram. The detector now reports variation in energy versus time for all the wavelengths simultaneously. Finally, the resulting interferogram is converted into the frequency domain applying a Fourier transformation. In this way, a transmittance or reflectance spectrum is obtained. What has been explained here is just the basic idea of the technique. In Apendix II, Fig.22 shows the specific beampath of the system.

3 Electron beam lithography on insulating substrates

In this section, we will focus our attention on EBL and its applicability to insulating substrates. As mentioned in the introduction, several methods have been developed to prevent charge distortions. Here, we will review and describe three of these fabrication methods on insulating substrates using conventional e-beam tools.

First, let us explain the origin of these charge distortions. In an e-beam exposure, when the primary electrons (PEs) of landing energy E_L strike the surface of the sample, they form a current I_{PE}. Then, secondary electrons (SEs), with energies < 50 eV, and backscattered electrons (BSEs), with energies ranging from 50 eV to E_L, are emitted in the vacuum leading to an electrom emission current I_E,

$$I_E = (\delta + \eta)\, I_{PE} \tag{1}$$

where δ and η are the secondary electron yield and the backscattered electron coefficient, respectively. The total electron emission yield is defined as

$$\sigma = \delta + \eta. \tag{2}$$

The dependence of σ on the landing energy of the incident electrons for typical, uncharged insulating materials is shown in Fig.10.

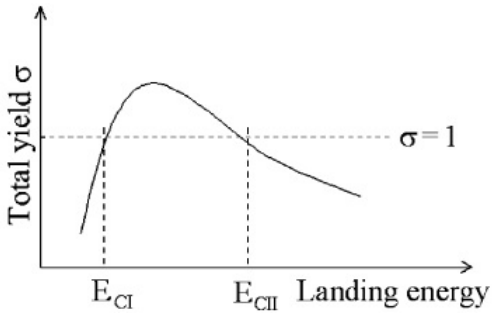

Figure 10: Total electron yield vs beam energy for a typical uncharged insulator [12]. The two energies where σ is unity, E_{CI} and E_{CII} are known as the first and second crossover energies. This curve is measured at the very begining of the irradiation process (just before charging affects the SE yield) by using a short pulsed primary beam.

According to the total electron emission yield approach [8], if the beam energy is larger than the second crossover energy, E_{CII}, a negative charge is injected into the specimen. If E_L is between E_{CI} and E_{CII}, a slight positive charging is expected. Since E_{CI} ranges from 10 eV-100 eV for insulators and the minimun acceleration voltage of standard EBL systems is 1 keV, hereafter positive charging will be considered if $E_L < E_{CII}$.

Therefore, when $E_L > E_{CII}$, a negative charge, Q, is injected into the sample. This charge induces a positive counter-charge (image-charge), Q_{im}, on the grounded sample holder,

$$Q_{im} = KQ,$$

where K is the electrostatic influence factor. This factor depends on the thickness and dielectric permittivity of the sample, and on the electrical characteristics of the media surrounding the sample[9]. The Q time-variation produces a displacement current, I_d, between the sample holder and the ground, given by

$$I_d = K\frac{\mathrm{d}Q}{\mathrm{d}t}. \tag{3}$$

Let us delve deeper into the effects of this surface potential. Let us consider V_S, the value of the surface potential produced by the built-up negative charge in the insulator. At the sample exit in the vacuum both SEs and BSEs are accelerated by the electric field induced by the trapped charge, in such a way that the energy distribution of emitted electrons at the insulator/vacuum interface corresponds to $[0, q\,(V_{ac} - V_S)]$ interval. Additionally, they hit the grounded inner walls of the specimen chamber with an energy ranging from qV_S to qV_{ac}, q being the electron charge. The interaction of the accelerated SEs and BSEs with the SEM inner wall materials leads to a secondary and backscattered electron emission.

These doubly-scattered electrons (from the sample surface and then from the SEM chamber-walls) form an additional electron source; they irradiate back the sample as well as the sample holder. The intensity of this source depends on V_S as well as the composition of the material constituting the SEM chamber. It is known that as soon as V_S exceeds a few kV, this intensity could reach a value as high as 30% of the PEs current intensity[10]. A part of these stray electrons, issuing from the additional electron source, impact the sample and again contribute to the re-exposure of the sample.

3.1 Charge dissipation methods

Now that the basis of the charging effect has been stated, we are in a position to introduce the different charge dissipation methods applied. Here, we will describe what every method takes advantage of, and the results will be presented in the next section.

Let us start with the simplest approach (from an experimental point of view), i.e., coating the insulating sample with the resist and running an exposure under rather unconventional EBL parameters. CE-EBL enables the patterning of nanometer scale structures, taking advantage of the crossover energies (Fig.10). In theory, in an exposure where the PEs have a landing energy equal to E_{CII}[7], no charge accumulation should occur, and therefore, no pattern distortions due to charging effects. However, determining E_{CII} could be challenging, or even impossible, depending on the system capabilities. The idea is that the determination of this acceleration voltage is simple, we know that when $E < E_{CII}$ there is a possitive charging whereas $E > E_{CII}$ leads to a negative charge accumulation. Working at different acceleration voltages and SEM imaging reveals the nature of the charge excess [11]. Although the idea is simple, the system may not allow an acceleration voltage variation precise enough to reach this point.

The second and third methods are the most commonly employed. In these methods, a conductive layer is coated either on top of or underneath of the resist layer. Although both techniques are different, they rely on the same principle. When a conducting layer is applied, eq.1 takes the form

$$I_E = (\delta + \eta)\, I_{PE} + I_L,$$

where I_L is the current flowing from the conducting layer to ground, the leakage current. Thus, the conducting layer drains the charge excess and charging is minimized or completely removed. Among the three methods employed here, using a conductive layer on top of the resist is the least EBL friendly. This approach requires an extra processing step (surface coating) and the use of EBL parameters that will ensure that the PEs go through the metal film and properly expose the resist. On the other hand, coating the substrate and then spinning the resist on top of the conducting layer makes the EBL exposure easy since, only standard EBL parameters are needed to expose the resist. Another advantage is that it eliminates the necessity of a post-exposure metalization of the surface, which makes the fabrication process faster.

A better insight of each method will be provided as we disscus the results obtained in the following section.

[7] As we mentioned before, working at E_{CI} is impracticable in EBL processes.

4 Results

Let us now discuss the different results found, but before, here we present the basic designs used while testing the different approaches. Fig.11

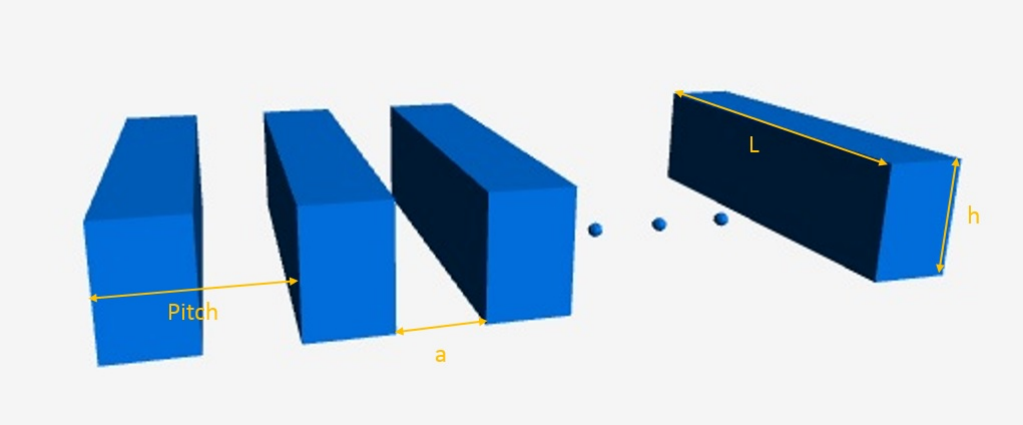

Figure 11: Grating designs. The figure shows the characteristic parameters of the structures: L is determined by the dimensions of the writefield, i.e, 100 μm, 200μm, etc, h is the thickness of the metal or resist layer, and a is the slits width. Different designs entail different values of a and/or the features pitch.

4.1 Critical energy electron beam lithography

Among the three methods here used, CE-EBL would be our first choice because its implementation seems straightforward. However, this is indeed the only approach that has failed in the attempt to fabricate nano-scale structures. The reason why this method failed was forseen during the sample preparation and nevertheless, we decided to test it. In order to better understand where we fail in properly implementing this method, let us review the whole process.

First thing required by this method is the determination of E_{CII}, as is described in [11], a variable magnification scanning method or "scan square" is the gauge used to determined this energy. Here, it is important to point out that E_{CII} does not need to be measured with high precision, ultimately is the acceleration voltage resolution of the electrons columns the constraint to this value.

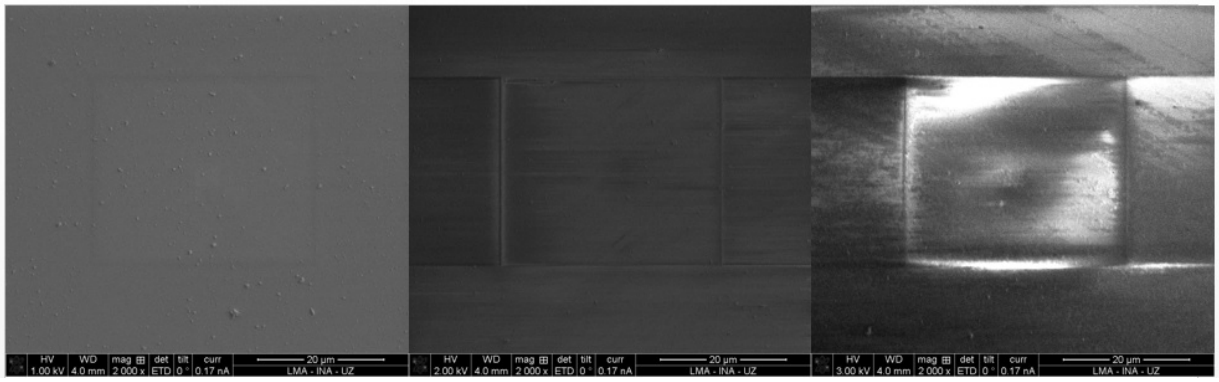

Figure 12: From left to right we present the variable magnification SEM images after dropping the magnification from x20000 to x2000 operating at 1 keV, 2 keV, and 3 keV , respectively, in order to find the second crossover energy (E_{CII}) of a 260 nm PMMA on quartz. The dark rectangles represent positively charged high-magnification regions, and the bright rectangles represent negatively charged regions. In the case of 1 keV, no voltage constrast is found visually .

The different SEM images taken during the variable magnification procedure are shown in Fig.12. These pictures are obtained using the SE detector and setting first the microscope to a magnification of x2000 (the magnification used by the system during EBL exposures) in live image mode during 20 seconds

and then, raised to x20000 for 10 seconds. Afterwards, the magnification is set back to x2000 and the images are captured. It was expected E_{CII} to be around 1 keV [11] and the left image in Fig.12 proves this to be true since no apparent voltage contrast is found between the different regions. On the other hand, in the two other images we find bright regions negatively charged, the repulsion of electrons in the surface increases the SE detector efficiency and therefore, appearing these regions brighter .

Once E_{CII} is measured we are in position to expose the designs. Although no charging effects appears at the magnification the EBL takes places (aprox. 1900), while focusing on the sample and working at high magnification charging appeared since we are not accurately at a $\sigma = 1$ point, making focus adjustments challenging. Nevertheless, we try to correct and focus the e-beam as much as possible and we proceed with the patterning step.

Fig.13 shows a cross section of one of the structures exposed applying this technique.

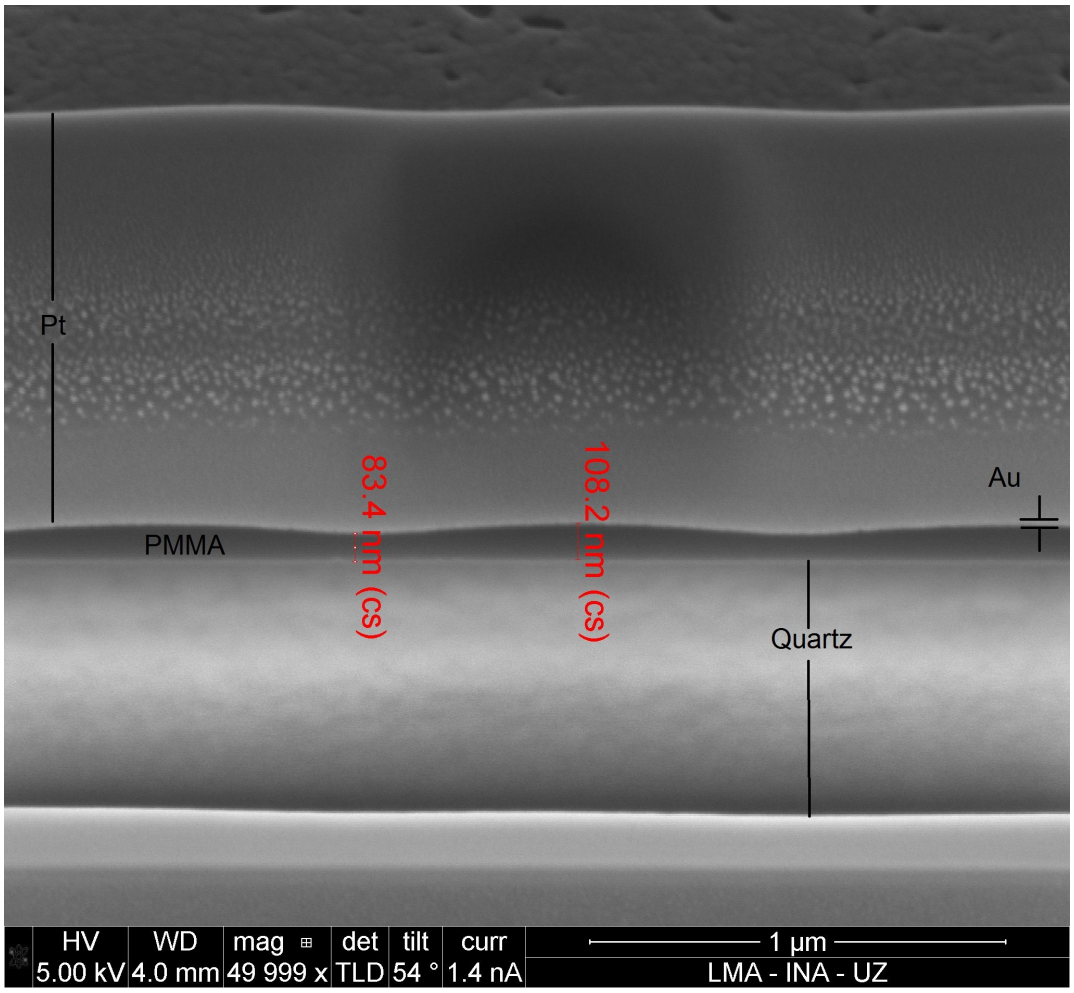

Figure 13: Cross section of a diffraction grating (100nm width, 500 nm pitch) CE-EBL exposesed.

We would have expected a well defined rectangular step sucession (Fig.11) however, we have sort of a wave profile. The reason is obvious, the mean free path of 1 keV electrons is aprox. 50 nm and, the resist layer thickness is 260 nm. Therefore, there is no an efficient exposure of the designs. PEs barely reach half of the resist layer and the high concentration of SEs and BSEs near the surface produces that wave-like profile. The shallower regions are where the PEs are aiming at meanwhile, the crests are results of SEs and BSEs. The resist layer thickness is the second main point to take into account in the application of this methods, we omitted it in the previous section to show how important this consideration is. In order to properly determine the optimum thickness we have to adopted the Kanaya–Okayama approximation for the electrons penetration depth:

$$R = 0.027 \frac{A E_L^{1.67}}{Z^{0.89} d}$$

where E_L is measured in keV, A is the atomic weight of the PMMA layer in g mol^{-1}, Z is the atomic

number and d is the density in g cm^{-3}. Using this formula, the electrons penetration depth in PMMA is 66.4 nm Thus, it is understandable that the exposures were unsuccesful.

4.2 Conducting layer approach

The conducting layer (CL) approach assures the charge excess dissipation through a metal layer and enables EBL patterning without charging distortions. Whether the conducting layer is either on top or underneath the resist layer is determined by the fabrication process. Usually, a conducting layer is spun on top of the resist when lift-off steps are needed along the fabrication process. In this case, the metal layer is removed afterwards and only represents a secondary step during the fabrication process. However, when the metal layer is underneath the resist this turns into a primary constituent of the fabrication process, where the resist layer acts as a mask that is transfered to the metal layer through different techniques like ion milling, RIE, etc.

4.2.1 Conducting layer on top of the resist layer

In the first experiments we adopted the conducting layer approach where the dissipation layer is on top of the resist. Based on [13], we decided to coat the resist with an Al layer; at a later stage, Au was also used for this purpose. Firstly, we tried with different Al thicknesses and an optimun thickness between 6 nm and 7 nm was found. Again, the thickness is determined by the dissipation capability of the metal layer. An Al layer thinner than 6 nm leads to charging effects on the surface whereas thickness thicker than 7 nm make more difficult the EBL. The thicker the Al layer the higher the dose has to be and therefore, higher currents are involved. The biggest problem of this approach is the overexposure of the PMMA layer. As it was introduced (Section 2) , the irradiation of the resist leads to the scission of the main chain due to radical processes. At an optimal dose, radicals recombine and form molecules with a molecular mass of about 5000 g mol^{-1}. However, an overexposure of the resist increase the radical formation and these undergo crosslinking so that molecules with higher molecular masses are obtained. The PMMA is turned into a negative resist.

After several attempts, an acceleration voltage of 5 keV and a current of 1.4 nA were found to provide the best results. A low acceleration voltage and a high current assure the electrons to pass through the metal layer and not overexpose the resist. In addition, an acceleration voltage of 3 keV at the same current leads to well defined structures. When the acceleration voltages used during EBL are this low we can talk about low voltage electron beam lithography (LVEBL). Although these parameters lead to well defined patterns, high doses are still required to properly expose the resist. Again, the thickness of the resist is a constraint and working with acceleration voltages lower than 3 keV will prevent the electrons of fully expose the resist, leading to the same effect as in Fig.11. Nevertheless, working under the conditions stated and once the critical optimal dose is found, the exposures produce well defined structures.

The next step in the fabrication process is the e-beam evaporation of a metal layer that will form the optical-devices and then, the lift-off of the resist layer. This second metalization only depends on the physical requirements of the optical devices however, we underwent problems during the lift-off process and we tried several thicknesses, ranging from 100 nm to 20 nm. Unfortunately, we never achieved a clean removal of the resist layer. In a lift-off process, the resist layer is removed through a wet etching process. Acetone and DMSO are the chemical removers employed for this purpose. From those two acetone is the most commonly used whereas DMSO is more harmful for the resist but also more powerful. Different combinations were tried during the lift-off process: immersion in acetone for more than one week, acetone and ultrasonic bath for several hours, immersion in DMSO for more than one week, DMSO and ultrasonic bath at 70^{o}C for several hours, etc. None of these experiments led to more than a partial removal of the resist.

There are several factors that contributes to facilitate a lift-off process. When a lift-off process is part of the fabrication process usually a bilayer resist structure is utilized during the EBL process. A resist with a low molecular weight resist layer is spun on top of the substrate followed by another layer with a higher molecular weight. As we stated, a lower molecular weight resist presents a lower optimal dose. Then, the EBL process takes place at the optimal dose of the upper resist layer leading to an undercut profile, after the development of the resist. Now, if a metal is evaporated, due to the undercut profile there is a spatial separation between the metal evaporated and the resist structure. Removal agents will attack through these undercut regions and a more effective removal of the resist takes place. However, we tackled the simplest lift-off aproach (only a resist layer) because in some cases it also provided total resist removal. Unfortunately, we only obtained a partial resist removal and did not have time to move

to a bilayer lift-off approach. Although we could not achieved a clean lift-off process and this defeated the main goal of this work, the partial removal of the metal made easier the SEM imaging of the results.

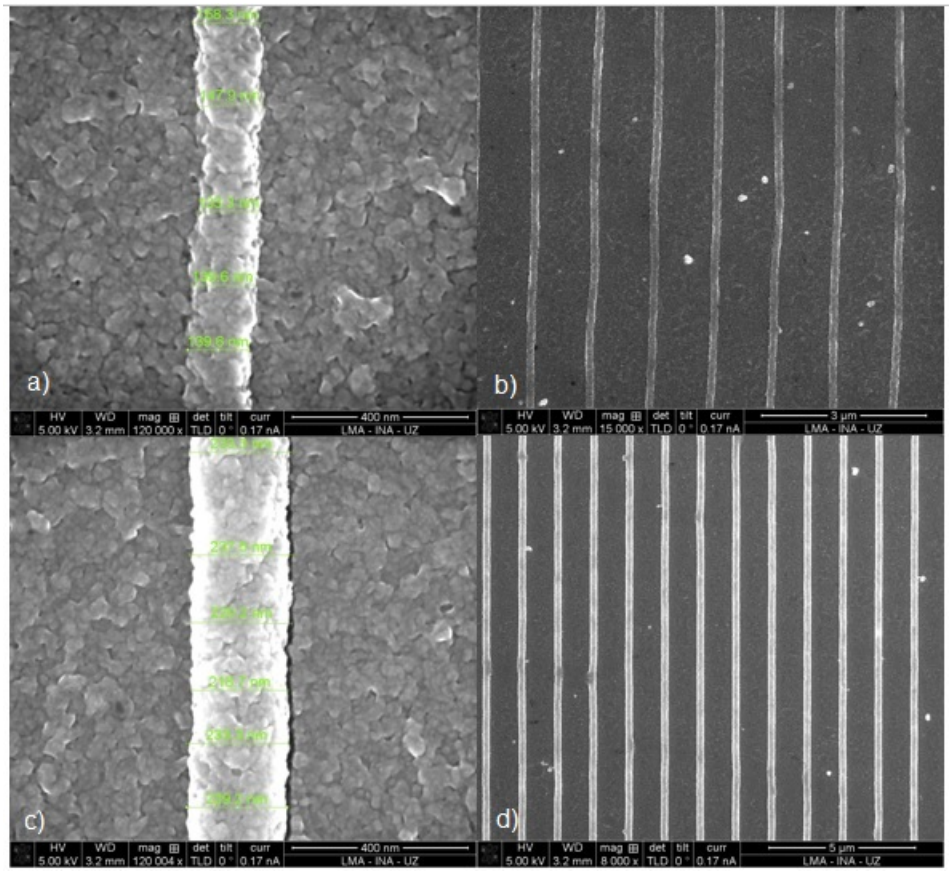

Figure 14: Lift-off results after EBL through the CL approach described above. In these experiments, a grating design with a pitch of 1.2 μm and variable slit width were exposed and a partial lift-off of 40 nm Al layer ensued. Fig.14 a)-b) show the limit case under the conditions discussed. In the design, the slit width is of 1.1 μm. In addition, not perfectly straight lines are obtained due to charging and interproximity effect. Fig.14 c)-d) show the design for a slit width of 1 μm. In this case, the profile of the slits are straight. Area doses in the range of 1.5 mC/cm^2 are involved in these exposures.

In Fig.14 some of the results obtained applying this method are shown. Although the lift-off was not successful, well defined structures are produced. In the images a) and b) we present the smallest feature dimensions obtained which barely reach 100 nm. This structure does not seem perfectly defined and some curvature is found in the slits. The reason is not other than the high dose used in the EBL process. Area doses in the order of 1.5mC/cm^{2}are required, which also highlight the charging distortions. In addition, working at this dose level inter-proximity effects gain more presence and that, is one of the reasons why a pitch of 1.2 μm was choosen. When the feature size increases, better results are obtained as is the case of images c) and d). Also, it can be noticed from Fig.14 that the design dimensions differ in 40 nm of those obtained. Since the lift-off process presented the problems stated, this may be one of the reasons for these thicker lines. However, it could also be due to an overexposure of the region. Either reason is plausible but, it is hard to distinguish which one is the dominant. Using lower doses to those shown produce structures affected by more imperfections so, we can not ultimately pinpoint why this problem has occurred.

4.2.2 Conducting layer underneath the resist layer

This variation produced the best experimental outcome. It is a simple approach but at the same time, limited; the method solely impresses the shape of the PMMA mask upon the CL or enables building

up extra layers on top of the CL[8]. Regarding EBL, the same conditions as in a standard Si samples are encountered and, no special parameters are needed during the exposures and no charging distortions are found. We would like to point out that from all the methods employed, this is the only one that totally eliminated any charge excess on the sample surface.

Whereas patterning on the resist layer is straightfoward, impressing the shape of the mask upon the metal layer could be challenging. The idea is, using the resist layer, to mill the metal layer through either RIE or ion milling. Again, the resist layer thickness is the main constraint, reactive ion etching is too aggresive to the resist used and it will remove it before the metal is milled. Notwithstanding, ion milling is compatible with the resist used and in fact, the resist thickness could play in our favor. As it was discussed in Section 2, when the structure is PMMA/Au, the Au ion milling rate is approximately the double of PMMA and in principle structures where the CL is the double in thickness than the PMMA layer, could be fabricated. However, it was noticed that different designs presented different ion milling ratios, i.e., the EBL patterning of different designs does not provide the same PMMA structure after development. Therefore, the ion milling of the resist may vary according to the design exposed. The reason why we opted to work with Au is because this material possesses an exceptional ion milling rate, larger than other materials availables like : Al, Ag, Ti, etc.

The usage of an O_2 plasma ashing is recommended for the total removal of the resist layer after the ion milling process. In this way, extra damage to the structures is avoided since not all the designs are milled at the same ratio and the O_2 plasma ashing removes the resist; yet, O_2 plasma ashing leads to oxidation of other materials. In this case, ion milling can be used to fully remove the resist layer.

Bearing in mind these limitations, this method provided far better results than the others. In what concerns the grating designs, this method is a reliable way to reproduce this sort of designs from pitches of 200 nm to 900 nm with a bar width of 100 nm and mostly any other combination with bar width ranging from 100 nm to 1000 nm and pitches ranging from 200 nm to 10 μm. A cross section of one of these designs is shown in Fig.15. In those SEM images we can see a cross section of a structure with a pitch of 2 μm and a bar width of 1 μm milled on a 50 nm Au layer. The bars show a slighly tilted edge profile which is due to the previous resist profile.

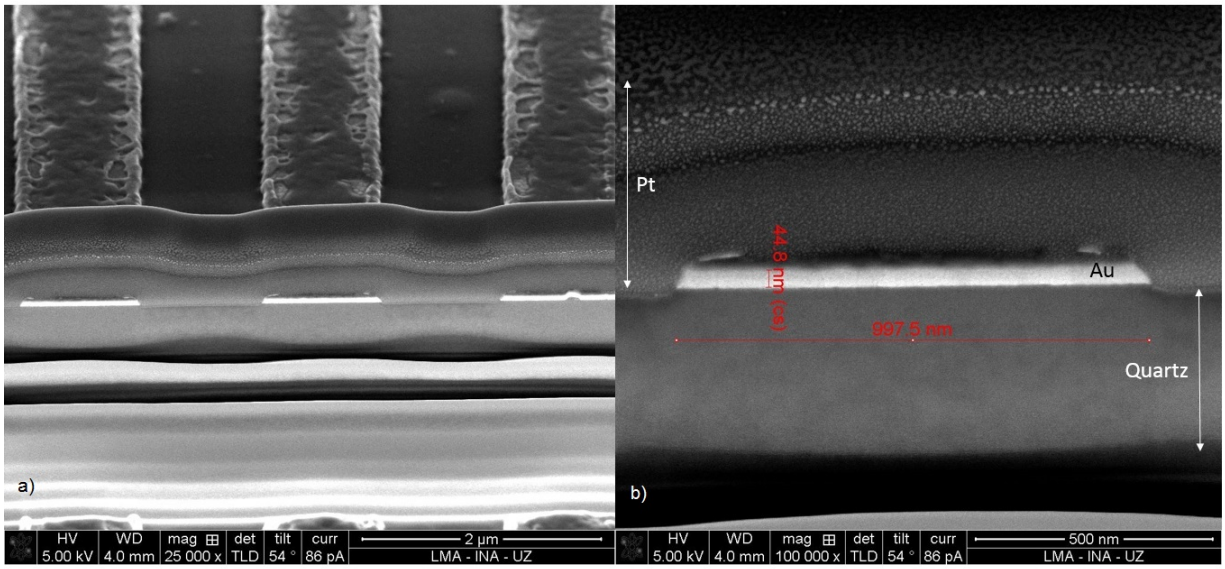

Figure 15: SEM images of a cross section of a metallic grating fabricated on a 50 nm thickness Au layer. Fig.15 a) shows the bars profile and the cross section of structure. Fig.15 b) shows in more detail the cross section region. The pitch of structure is 2 μm and the bar width of 1 μm

Since this method was successful we decided to further test it in thicker Au layers. In order to do so, we develop a new design consisting in arrays of different geometric feautrures as : triangles, squares, circles and rectangles. Arrays of triangles, circles, and squares were a bit more problematic so we decided to focus in subwavelength rectangular appertures arrays becasuse of their particular transmission response. Inspired by Ref.[14] we focused our efforts in rectangular arrays of vertical and horizontal pitch of 1.6

[8] Here, we will only focus in transfering the PMMA mask in to the CL, building up another layer could be done depositing whatever material is needed and removing the PMMA through a wet etching process, i.e., lift-off process.

μm and 250 nm, repectively. The rectangules side L (Fig.11) was kept constant at 800 nm whereas the rectangle width ranged from 10 nm to 90 nm. The extrem cases of these designs are shown in Fig.16.

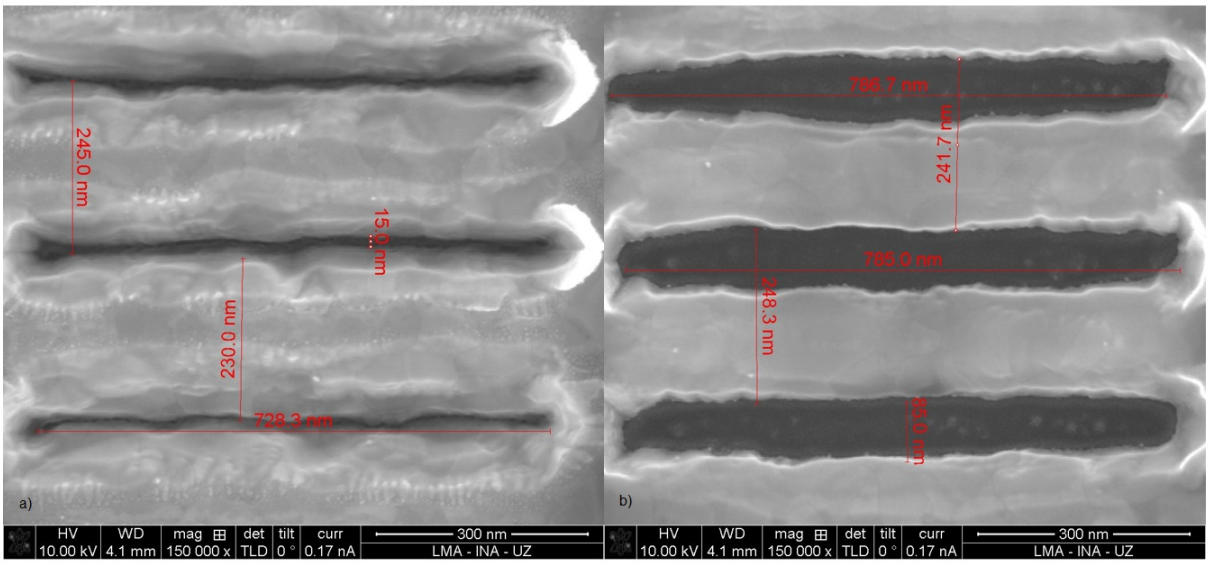

Figure 16: These SEM images show the results of our attempt of patterning even smaller features. The designs patterned this time were rectangle arrays whith a vertical and horizontal pitch of 1.6 μm and 250 nm respectively. Image a) represents the smallest structure achieved through this method where the rectangle width goes down to 15 nm. Image b) shows the same design for a larger width of 85 nm.

Surprisingly, we were able to pattern structure down to a rectangle width of 15 nm. In order to corroborate this value, a cross section of the sample was done. Fig.17 shows the cross section for both 10 nm and 50 nm rectangle width arrays. Fig.17 a) shows a slit width of 11.5 nm in 260 nm thickness Au layer, the smallest structure ever made at the INA facilities. We have to point out that the minimun resolution that EBL can provides is of 10 nm (or slighly under this value) working with conducting substrates under very specific conditions, employing dedicated e-beam writing systems, and utilizing special resists as HSQ. Here, we provided a method that closely match that accuracy level in an insulator substrate and yet, no special equipment and/or material is required and we are even working with quite thick resist layers. Of course, the cost of such a narrow slits is a not well defined profile; as the width increases the profile definition improves. Fig.17 b) shows a cross section of a design with a slit width of 50 nm and an Au layer thickness of 160 nm.

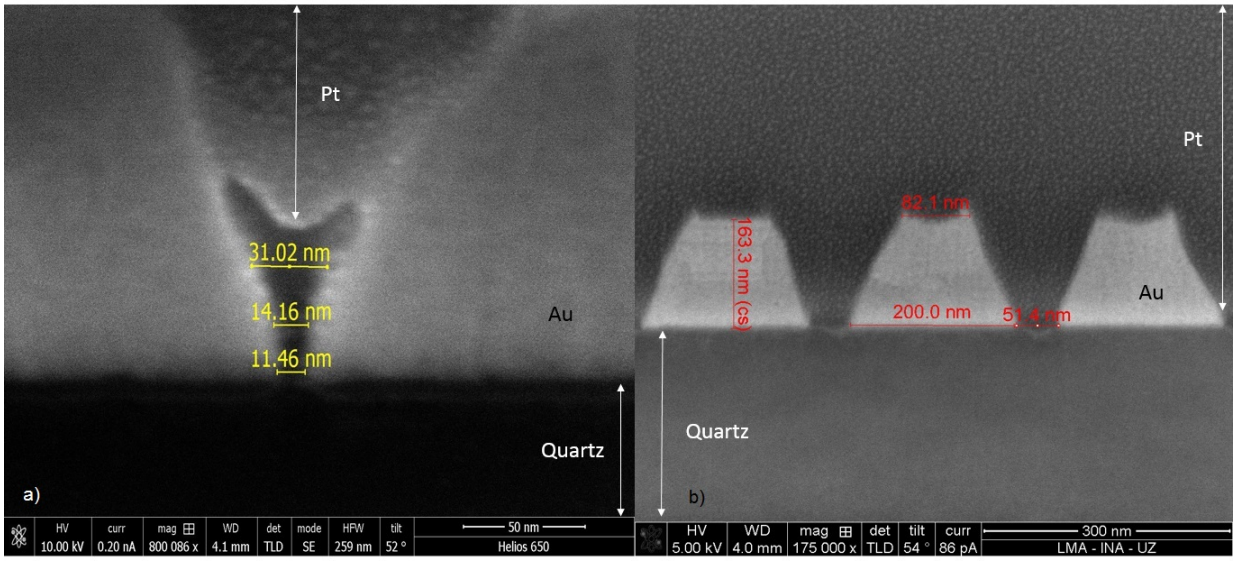

Figure 17: SEM images of a) a cross section of a rectangules array of 10 nm width and b) a cross section of a rectangles array of 50 nm width. The Au layer thickness is of 160 nm.

The cross section of these designs shows a tilted profile as discussed previously. In these cases, the effect is larger since the metal layers are thicker. In addition, we can notice a shallower quartz regions in the bottom of the slits which means that the ion milling has slightly attacked the substrate. Furthermore, some of the bars shows a curvy top which is just an effect produced by the resist that is harder to remove at the edges of the features. These tilted profiles will have negative repercussions upon the transmittance of the designs but, they are ultimately due to the resist procesing. A reduction in the developing time will improve the resist mask profile.

Fig.18 presents transmittance and reflectance of the rectangular structures discussed in Fig.16 and Fig.17. As can be noticed, a narrow peak appears near to what it could be ElectroMagnetic (EM) modes bound to the metal surface called Surface Plasmon Polariton (SPP). SPPs are EM excitations of a coupled state between phothons and an plasma oscillations propagating at the interface between a conductor and a dielectric, evanescently confined in the perpendicular direction. In this case, the peak is close to what theoretically would be predicted as the first SPPs in the interface air/metal, $\lambda_{spp} \geq np$, where n is the air refracction index and p is the vertical pitch, 1.6 μm. The larger the rectangule width is the larger the transmittance gets. At a rectangle width of 20 nm and 50 nm the effect is small however, at 85 nm the transmittance grows up to 20% and the shape is very narrow, which is why we think this may be due to a SPP.

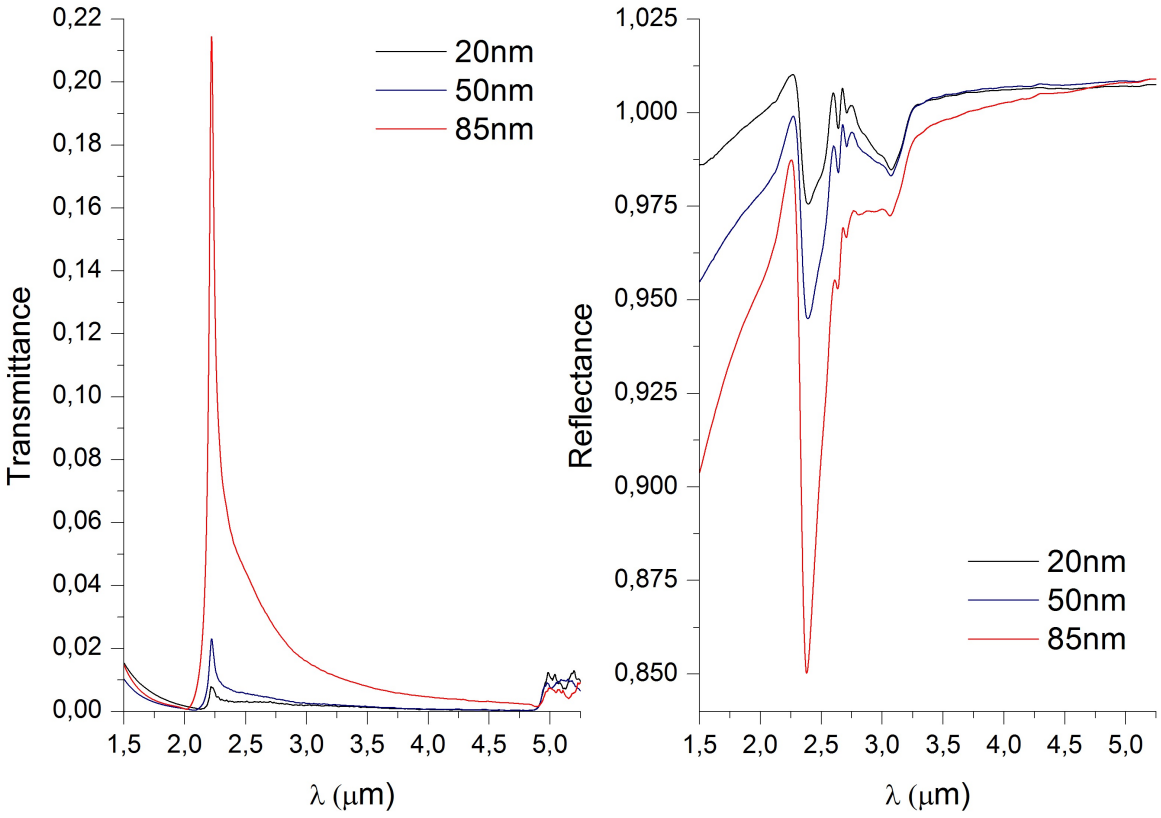

Figure 18: FTIR measuraments of the transmittance and reflectance of the designs shown in Fig.16 and Fig.17, where the Au layer thickness is of 160 nm. In the case of transmittance measurements the reference is measured on a quartz sample and in the Au sample surface in the case of reflectance measurements. Each series is characterized by the rectangle width of each design. As the width grows bigger so does the transmittance of the structure.

In addition, further designs were exposed in a thicker Au layer (200 nm), the results are shown in Fig.19.

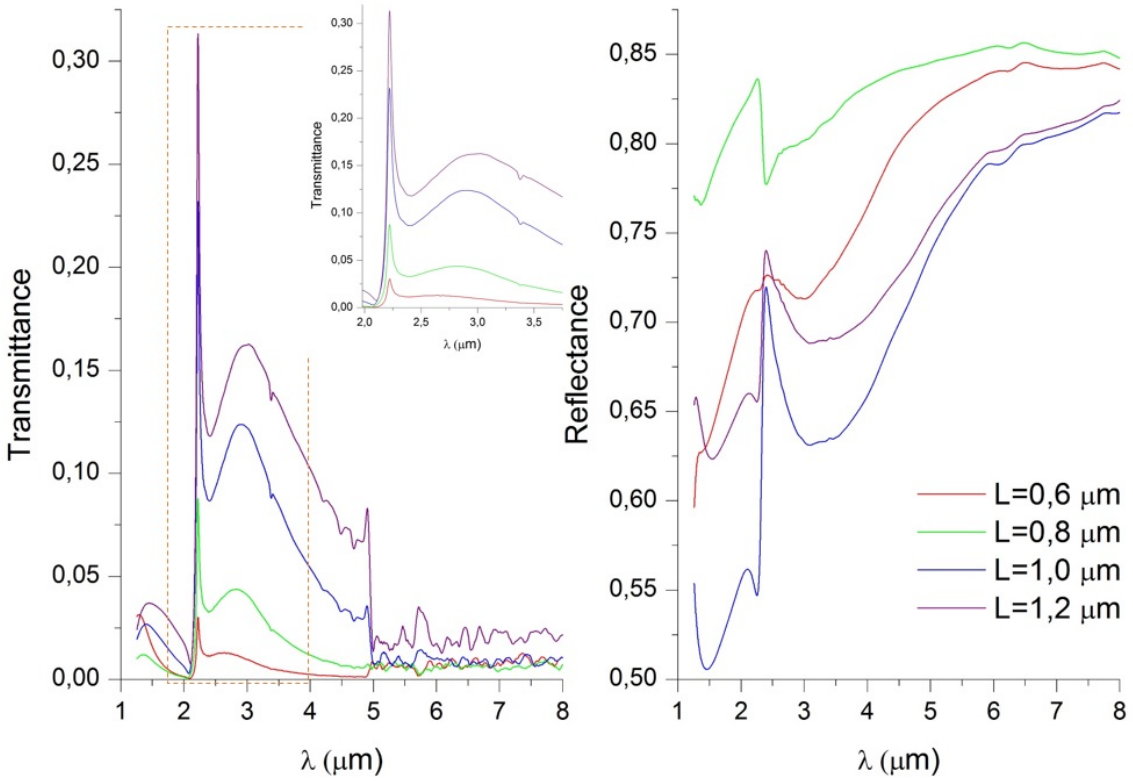

Figure 19: FTIR measuraments of the transmittance and reflectance of rectangules arrays where the width is 50 nm and L (Fig.11) ranges from 600 nm to 1.2 μm, where the Au layer thickness is of 200 nm. In the case of transmittance measurements the reference is measured on a quartz sample and in the Au sample surface in the case of reflectance measurements. There is a zoom-in image of the region enclosed by the red dashed lines.

Two types of transmission resonances can be distinguished: very narrow transmission peaks appearing at a wavelength close to the value of the pitch and wider peaks emerging at longer wavelengths. The latter are the result of waveguide modes propagating in the inside of the rectangular slits, this resonances are called Fabry-Perot resonances because of its simailarity to a Fabry-Perot resonator response. As we could expect, since the vertical pitch does not change, the possible SPPs peak occurs at slightly the same wavelength as in the case presented in Fig. 18. Furthermore, it seems that the Au layer thickness increase has led to the appearance of far right resonance peak, what we think a Fabry-Perot resonance is. As the wavelength increase, the EM mode propagating in the surface becomes leaky. This is due to the fact that in the long wavelength limit metal behave has perfect electric conductors, so that the modal fields do not penetrate into the metal.

As follows from Fig.19, the larger the L side the higher is the transmision efficiency of the structure and the narrower both peaks get. However, we cannot certainly say that the peaks above discuss correspond to SPPs or Fabry-Perot resonances. Further structures with different vertical pitch values should be fabricated. If what we have stated above is true, then the FTIR measurements of these structures will lead to a horizontal shift of the transmission peaks. That would be the last test needed to certainly assured what has been said. Unfortunately, system mechanical failure has prevented us to carry out this last test.

5 Conclusions

Along this work we have presented 3 approaches to avoid charge distortions while EBL patterning on insulating substrates. Although no all of them have led to the results expected, we have reviewed and analized the three of them.

In the case of CE-EBL, this has been shown to be the easiest to implement. However, as we have already foreseen, the resist thickness is a major limitation and EBL patterning was unsucccesful. Nevertheless, the implementation process has been presented and working with a different resist results as the one presented in [11] could have been obtained.

On the other hand, the method that implies the use of a CL have shown better results. Between the two CL approaches here explained, the used of a CL on top of the resist has shown big limitations. The conditions under EBL takes place rather contribute to charge distortions than avoid them since high doses of low energy electrons are needed to properly expose the resist and to pass through the CL. In addition, the lift-off approach presented was not the most appropiate for the purposes required but, non additional resist with different molecular weights were available to implement a bilayer approach.

Fortunately, the experiments where a CL was place underneath the resist showed the best results (by far) and several designs were tested finding reproducible structures with a feature size below 12 nm. In which only concerns with EBL, it has not been found any signals of surface charging no matter how much we raised the magnification and the patterns are not affected by this either. Specifically, we want to bring up the importance of the resolution achieved through this method. Under the best ideal EBL conditions working with Si substrates, the minimum resolution that could be obtained is around 9 nm to 10 nm. In order to achieve such a small features, the EBL requires a very thin layer of HSQ resist and EBL dedicated systems. Here we are working with an insulator substrate, we are using a thick PMMA (the most common EBL resist) layer, a multi-purpose EBL system and yet, we have obtained a resolution down to sub-12 nm. Probably, using a resist that allows thinner layers and finding the best development times, we could produce perfectly defined structures down to a 10 nm resolution.

On the other hand, the used of a CL underneath the resist layer has been proved to be an alternative method to ion beam lithography in the fabrication of subwavelength metal apertures on insulating substrates. FTIR transmittance and reflectance measurements have shown how these subwavelength apertures leads to interesting transmission peaks. Increasing the rectangles width keeping the vertical pitch constant in a 150 nm Au layer led to an increased in the transmittance response of structures up to a 22% at the maximum peak. Similarly, increasing the rectangles length keeping the vertical pitch constant in a 200 nm Au layer led to a 35% transmittance peak and at the same time, wider peaks at longer wavelength have appeared.

In conclusion, from all the method discussed above the usage of a CL underneath the resist layer has shown the best throughput and is the only one that has succesfully eradicated any charge distortion.

Appendix I

In this appendix we will review the method applied to dertermine the Au, Al, and PMMA ion milling rates, as well as the PMMA O_2 plasma ashing rate.

For that puporse, we took two quartz samples, coated them with a 150 nm metal layer (Al and Au, respectively), and then spun PMMA on top of it. A 200μm×400μm rectangle was patterned using EBL and then they were developed. Profilometer measurements (Fig.20)

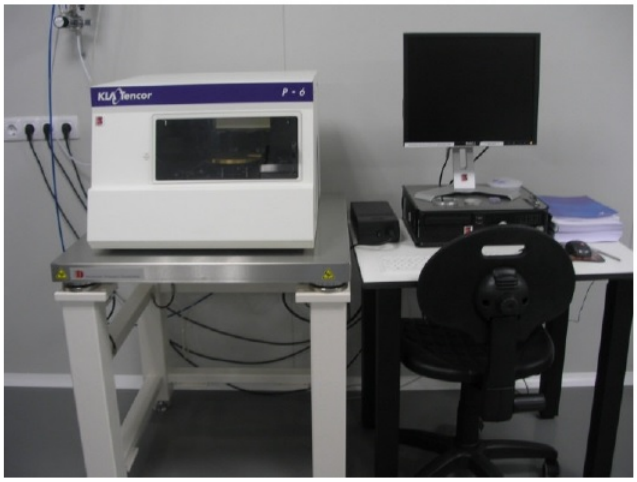

Figure 20: Profilometer system.

determined the resist thickness layer to be approximately 260 nm. An ion milling step followed. Both samples were placed in the system together and additionally another metal strip was placed on top of them acting as a shadow mask, Fig.21.

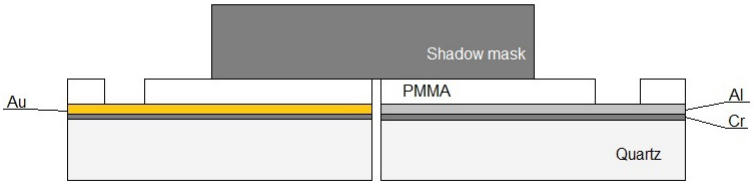

Figure 21: Sample positioning.

After 5 minutes of ion milling, the sample is taken back to the profilometer. The shadow mask allows the measurement of the PMMA ion milling rate, 10nm/min. Similarly, a profilometer measurement of the rectangular exposed area is compared to itself after 10 minutes of O_2 plasma ashing. In this way, the PMMA O_2 plasma ashing rate of 12.5 nm/min was measured. Finally, taking into account the PMMAO_2 plasma ashing rate, the resist layer was completely removed and new profilometer measurements were done. These measurments determined that the ion milling rates of Au and Al were 22.5 nm/min and 6 nm/min, respectively.

The resist supplier states that a hardbake of the resist (130 degrees, 1 minute) slightly increased the O_2 plasma ashing rate. Following the procedure above described no remarkable improvements were found. Therefore, the hardbake of the sample was discarded, as it entails more disadvantages than improvements.

Apendix II

In this appendix we present the optical beampath of the Hyperion 2000 system.

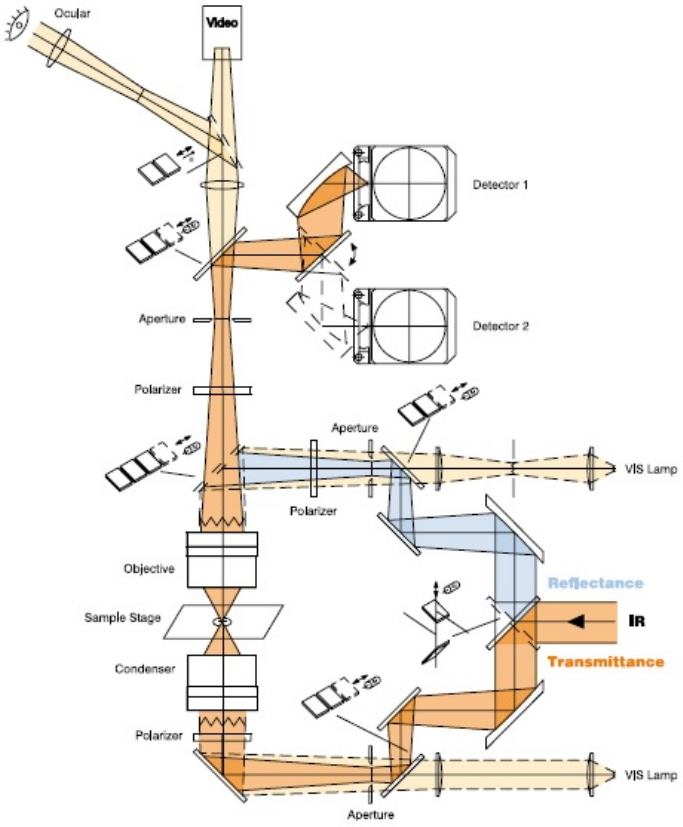

Figure 22: Optical beampath of Hyperion 2000

References

[1] B.D. Myers, V.P. Dravid, Nano Lett. 6 (2006) 963.

[2] S. Choi, M. Yan, L. Wang, I. Adesida, Microelectron. Eng. 86 (2009) 521.

[3] Y. Kanamori, H. Kikuta, and K. Hane, Jpn. J. Appl. Phys., vol. 39, no. 7B, pp. L735–L737, Jul. 2000.

[4] Y. Kanamori, M. Ishimori, and K. Hane, IEEE Photon. Technol. Lett., vol. 14, no. 8, pp. 1064–1066, Aug. 2002.

[5] A. G. Lopez and H. G. Craighead, Opt. Lett., vol. 23, no. 20, pp. 1627–1629, Oct. 1998.

[6] Resist datasheet. `http://www.allresist.com/wp-content/uploads/sites/2/2014/02/allresist_produktinfos_ar-p630-690_englisch.pdf`

[7] Wayne M. Moreau. Semiconductor Lithography: Principles, Practices and Materials. Plenum Press, New York 1988.

[8] D.C. Joy, Scanning 11 (1989) 1.

[9] R. Coelho, B. Aladeniz, B. Garros, D. Acroute, P. Mirebeau, IEEE Tran. Dielectr. Electr. Insul. 6 (1999) 202.

[10] M. Belhaj, O. Jbara, M.N. Filippov, E.I. Rau, M.V. Andrianov, Appl. Surf. Sci. 177 (2001) 58.

[11] J. Joo, B.Y. Chow, J.M. Jacobson, Nano Lett., 2006, 6 (9), pp 2021–2025

[12] S. Fakhfakh, O. Jbara, M. Belhaj, Z. Fakhfakh, A. kallel, E.I. Rau, Nucl. Instr. and Meth. in Phys. Res. B. 197, pp. 114-127 (2002).

[13] Volume PM39, Handbook of Microlithography, Micromachining, and Microfabrication: Volume 1 P. Rai-Choudhury, Editor

[14] Garcia-Vidal et al. Rev. Mod. Phys., Vol. 82, No. 1, January–March 2010

[15] Barbara, A., P. Quemerais, E. Bustarret, and T. Lopez-Rios, 2002, Phys. Rev. B 66, 161403.